Symmetric and Asymmetric Meniscus Collapse in Wetting Transition on Submerged Structured Surfaces

ARTICLE *in* LANGMUIR · DECEMBER 2014

Impact Factor: 4.46 · DOI: 10.1021/la503465q · Source: PubMed

7 AUTHORS, INCLUDING:

Yahui Xue
Peking University
15 PUBLICATIONS **110** CITATIONS
SEE PROFILE

Peng Xi
Peking University
89 PUBLICATIONS **753** CITATIONS
SEE PROFILE

Hao Lin
Rutgers, The State University of New Jersey
55 PUBLICATIONS **717** CITATIONS
SEE PROFILE

H. L. Duan
Peking University
103 PUBLICATIONS **2,187** CITATIONS
SEE PROFILE

Langmuir

Article

pubs.acs.org/Langmuir

Symmetric and Asymmetric Meniscus Collapse in Wetting Transition on Submerged Structured Surfaces

Pengyu Lv,[†] Yahui Xue,[†] Hao Liu,[†] Yipeng Shi,[†] Peng Xi,[‡] Hao Lin,*[,§] and Huiling Duan*[,†]

[†]State Key Laboratory for Turbulence and Complex System, Department of Mechanics and Engineering Science, CAPT, IFSA Collaborative Innovation Center of MoE, College of Engineering and [‡]Department of Biomedical Engineering, College of Engineering, Peking University, Beijing 100871, China

[§]Mechanical and Aerospace Engineering, Rutgers, The State University of New Jersey, 98 Brett Rd., Piscataway, New Jersey 08854, United States

Supporting Information

ABSTRACT: The wetting transition from the Cassie−Baxter to the Wenzel state is a phenomenon critically pertinent to the functionality of microstructured superhydrophobic surfaces. This work focuses on the last stage of the transition, when the liquid−gas interface touches the bottom of the microstructure, which is also known as the "collapse" phenomenon. The process was examined *in situ* on a submerged surface patterned with cylindrical micropores using confocal microscopy. Both symmetric and asymmetric collapses were observed. The latter significantly shortens the progression of the metastable state prior to the collapse when compared with the former and hence may affect the lifespan of superhydrophobicity. Further experiments identified that asymmetric collapse were induced by impurities due to prior use of the structure. The problem is thus of broad relevance, since endurance through cycles is a practical requirement for these functional surfaces. Finally, the use of hierarchical structures is proposed as a remedy. The embedded self-cleaning mechanism serves to effectively remove the impurities, so as to avoid the triggering mechanism for asymmetric collapses.

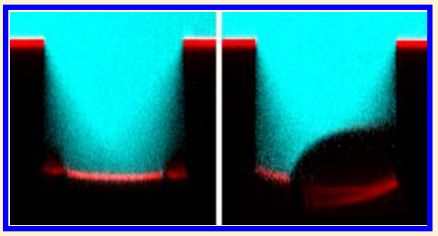

INTRODUCTION

Superhydrophobicity has attracted great attention due to their broad applications in both engineering and sciences.[1−10] Air pockets trapped in the surface-embedded microstructures in the Cassie−Baxter (CB) state[11] play a key role in realizing a large effective contact angle for a droplet deposited on the surface and a low hysteresis for liquid moving on the surface. However, the liquid−gas interfaces of the air pockets are subject to instabilities induced by various factors including vibration,[12] evaporation,[13−15] air diffusion,[16−18] pressurization,[19,20] geometrical parameters,[21,22] electrowetting,[23,24] and impact,[25,26] leading to the fully wetted Wenzel (W) state[27] and the failure of superhydrophobicity. The dynamic process of wetting transition from the CB to the W state has been captured by various techniques, such as light reflection,[16,18,28−30] optical diffraction,[31,32] X-ray,[33] and confocal microscopy.[17,34−38] Understanding this phenomenon is critical for the regulation and improvement of CB-based superhydrophobicity and conducive to the design of underwater structured surfaces with enhanced lifetime. Previous analyses on the CB−W transition focused on the energy barriers between the states from an energy point of view[39−44] and the critical pressure at which the liquid−gas interfaces depin from the top edge of the microstructures using a force-balance analysis.[45−48]

The CB−W transition follows different mechanisms for a droplet deposited on a surface and a submerged, structured superhydrophobic surface. The former is often correlated with evaporation,[28,35] whereas the latter contains several phases, which are illustrated in Figure 1. Initially, the water−air interface pins at the top corners of the microstructure in the CB state (Figure 1a). With an increase of the hydrostatic pressure, the contact angle along the sidewall increases to reach the advancing contact angle, θ_a, with the meniscus still pinned (Figure 1b). The interface subsequently depins and sags into the pore interior, leading to the metastable state (Figure 1c). Because of air diffusion into the water bulk, the meniscus advances toward the bottom, resulting in an eventual touchdown. The manner of the touchdown follows two possible configurations, namely, symmetric and asymmetric (Figures 1d1 and 1d2). Finally, the pore will be fully filled with water, accomplishing transition to the W state (Figure 1e). The first three phases, i.e., the process shown in Figure 1a−c, have been thoroughly investigated in a recent study by us;[49] we provided the first controlled and detailed quantification of the metastable state during the transition via confocal microscopy *in situ* and discovered a similarity law and a time scale governing the lifespan of the metastable state under various ambient conditions. In particular, variation in the hydrostatic pressure is important for applications such as drag reduction on a submerged surface and is less pertinent to a deposited droplet. Images of these phases can be found in ref 49.

Received: August 28, 2014
Revised: December 27, 2014

DOI: 10.1021/la503465q
Langmuir XXXX, XXX, XXX−XXX

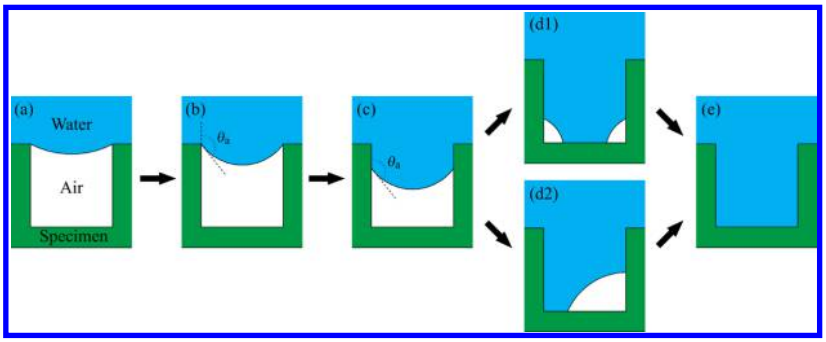

Figure 1. Phases of wetting transition from the CB to the W state. (a) The CB state showing a pinned meniscus. (b) The CB state with the contact angle along the sidewall reaching the advanced configuration. (c) Depinning and the metastable state, which advances due to air diffusion. (d1, d2) Meniscus collapse (touchdown) with a symmetric and an asymmetric configuration, respectively. (e) The fully wetted W state.

In this work, we continue our efforts to tackle the complex CB–W transition process for submerged structured surfaces and focus on the last stage shown in Figures 1d1 and 1d2, namely, the collapse. This stage succeeds the metastable state and is defined by the contact of the liquid–gas interface with the bottom of the microstructure. In many cases, this process is pictured to be symmetric in geometry about the center of the meniscus and the supporting structure (Figure 1d1).[39,50−52] Recently, asymmetric collapse with liquid finger and vapor bubble formation (Figure 1d2) has also been proposed by both continuum and atomistic simulation studies.[53,54] However, a direct, *in situ* observation has been in general absent and is the pursuit of the current work.

Following our prior efforts,[20,49] we use laser scanning confocal microscopy to investigate the collapse process and capture the collapse configurations on surfaces patterned with cylindrical micropores. We present the first detailed observation of both symmetric and asymmetric collapses *in situ*. The results indicate that asymmetric collapse can significantly shorten the progression of the metastable state and hence affect the lifetime of superhydrophobicity. An impurity-base mechanism is proposed to explain asymmetric collapse, and extensive experiments were performed to validate the hypothesis. Importantly, those impurities derived from prior uses of the surfaces, which are unavoidable for devices in practical applications. On the basis of this understanding, we propose that the use of hierarchical structures can effectively address the problem, by employing the self-cleaning mechanism on the pore bottom. In combination with our previous work,[20,49] we collectively provide a complete description of the CB–W transition on submerged microstructured surfaces.

EXPERIMENTAL METHODS

The experimental setup is shown in Figure 2a. Samples patterned with cylindrical micropores were obtained by photolithography and deep reactive ion etching on silicon substrates, which were further coated with self-assembled monolayers of fluorosilanes to achieve hydrophobicity. The microstructure may be of a single level (Figure 2b) or may possess hierarchical structures on the pore bottom (Figure 2c). The solid fraction of our sample is around 0.60. The advancing contact angle of water on the structured sample surface was measured using a SL-200B contact angle measuring instrument (Kino, Shanghai Nuona Equipment, Shanghai, China) to be 132 ± 2.3°. Therefore, strictly speaking, the surface is not superhydrophobic as the angle does not exceed 150°. However, the results to follow do not lose generality and may apply to both structured hydrophobic and superhydrophobic surfaces. (For example, superhydrophobicity can be achieved on the current sample by simply decreasing the solid fraction from 0.60 to 0.27, according to the Cassie–Baxter equation.[11] This change in the solid fraction does not alter any of the dynamics within a single pore as presented below.) A specimen was mounted on the bottom of a sealed plexiglass box and gradually submerged in deionized water, labeled by Rhodamine B. In order to capture the last stage of the wetting transition, i.e., the process of meniscus collapsing toward the pore bottom, we applied a hydrostatic pressure of 50 kPa above the atmospheric pressure via the inlet nitrogen pressurization and then maintained the pressure to allow full development of wetting transition from the Cassie state to Wenzel state. All experiments were carried out at a constant temperature of 22 °C and a constant humidity of 60% RH. After each experiment, the sample was dipped into ethanol for at least 1 day to wash away the residual rhodamine-labeled water in the micropores and then was blown dry by a nitrogen flow.

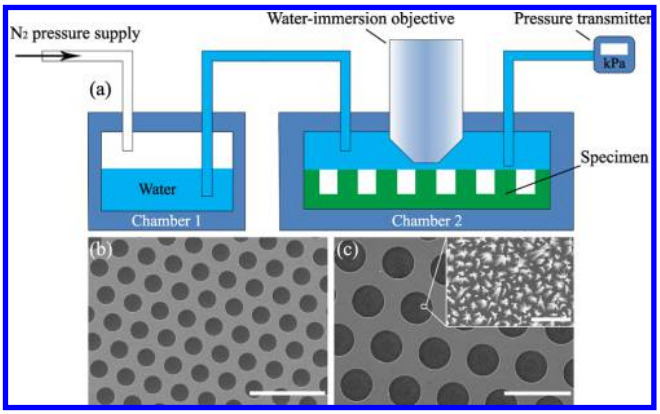

Figure 2. (a) Schematics of the experiment setup. Hydrostatic pressure over the specimen is supplied by compressed nitrogen up to 1.5 atm and monitored by a pressure transmitter at the sample surface. The meniscus profile is measured by confocal microscopy. (b) Scanning electron microscopic (SEM) image showing the pore-patterned sample in the absence of hierarchical structures. Each pore has a radius of 25 μm and a depth of 40 μm. The scale bar is 200 μm. (c) SEM image of a pore-patterned sample with hierarchical structures on the pore bottom. Each pore has otherwise the same dimensions as that shown in (b). The scale bar is 100 μm. The inset shows detailed morphology of the pore bottom with a scale bar of 2 μm.

Real-time optical observation was carried out to monitor the movement and deformation of the menisci using a Carl Zeiss laser scanning confocal microscope (LSM 710, Carl Zeiss, Germany) with a 20× water immersion objective (NA = 1.0, WD = 1.8 mm). Time-series images were recorded in two imaging modes, i.e., 2D line scan mode and 3D frame scan mode. 2D line scans across the pore diameter take advantage of the axisymmetric pore shape and can be used to obtain full knowledge of the location, curvature, and contact angle of the moving meniscus. 3D configuration of the meniscus can be reconstructed by a series of Z-stack images and gives the global information on the wetting transition and the collapse. Each scan, in

DOI: 10.1021/la503465q
Langmuir XXXX, XXX, XXX–XXX

both 2D and 3D modes, beginning from below the bottom of the pore until reaching above the specimen surface was controlled to consume less than 30 s. This time scale is much smaller than that of air diffusion, which we identify as the main mechanism driving meniscus progression.[49] Thus, the change in the meniscus shape during each scan was negligible. The time-series images are integrated and compiled as an animation to show the whole dynamic progress visually.[55] Unless otherwise noted, the following experiments were performed with single-level structures such as that shown in Figure 2b. Results with hierarchical structures such as that shown in Figure 2c are presented later.

RESULTS AND DISCUSSION

Both symmetric and asymmetric collapses of the water−air interface are shown in Figure 3. The superposition of the fluorescence (cyan) and reflection (red) images clearly illustrates the morphology of the water−air and silicon−air/water interfaces. The first and second rows denote the symmetric and asymmetric collapse, respectively. Figures 3a and 3e are line scans taken immediately before the collapse, and Figures 3c and 3g are immediately after. In both collapse configurations, the water−air interfaces were similar prior to the collapse, which exhibited a symmetric sagging about the central axis of the micropore. However, the dynamic advance toward the pore bottom differed from each other. For the case of a symmetric collapse, the air column progressively became thinner and thinner (Figure 3a) as air diffused into the water. The meniscus advanced to the bottom gradually, which eventually induced Newton's rings (Figure 3b), the interference pattern created by the reflection of light from the meniscus and the pore bottom. This means that the distance between the meniscus and the pore bottom was on the same order of magnitude of the wave length of the laser, which was 488 nm in our experiment. Then the meniscus suddenly contacted the pore bottom concentrically (Figure 3c), leading to a symmetric collapse. The triple contact line continued to spread out until the fully wetted Wenzel state was accomplished. Although the image in Figure 3d appears concentric with the pore bottom, the spreading usually becomes eccentric while approaching the pore side walls (not shown). For the case of an asymmetric collapse, the center of the meniscus was much farther away from the pore bottom immediately before the occurrence of collapse (Figure 3e). The triple contact line on the inner side wall suddenly touched the bottom of the pore (Figure 3g) on a time scale shorter than the frame interval, leading to an asymmetric collapse. Subsequently, the contact line on the pore bottom spread until fully wetting the pore. This asymmetric collapse was not induced by a direct contact of the meniscus with the bottom due to its advancing such as in a symmetric collapse. We ascribe this phenomenon to the loss of interfacial stability triggered by impurity-induced local microdroplet on the pore bottom, which we substantiate with further experiments below. 3D movies of both symmetric and asymmetric collapses animating the dynamic process are included in the Supporting Information.[55]

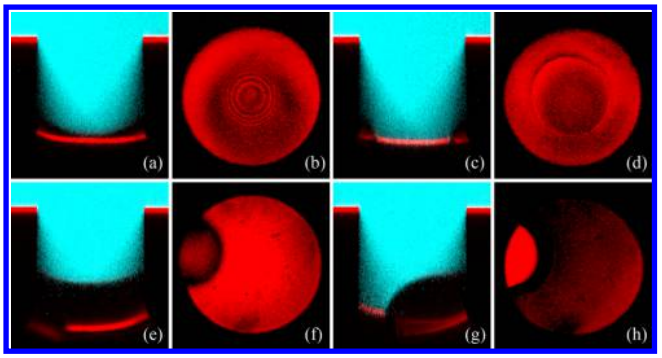

Figure 3. Symmetric (a−d) and asymmetric (e−h) collapse of the water−air interface. (a) and (e) are side-view line scans taken immediately before the collapse; (b) and (f) are corresponding top views of the pore bottom. (c) and (g) are side-view line scans taken immediately after the collapse; (d) and (h) are the corresponding top views. In (b), Newton's rings are observed due to the thin air lens formed between the meniscus and the pore bottom. In (f), a characteristic collapse-triggering ring is observed.

A total of 54 experiments with pressure applied between 15 and 50 kPa have been performed under the direct observation of confocal microscopy. Among these, 6 exhibited symmetric collapse and 48 exhibited asymmetric collapse. Without exception, the partial circle (Figure 3f) was always observed prior to any asymmetric collapse. Conversely, it was always absent for all symmetric collapse. On the basis of this strong correlation between the partial circle and asymmetric collapse, we hypothesize that these patterns are microdroplet condensations facilitated by local impurities. Indeed, we have captured the droplet-like features in Figure 4. These microdroplets were mostly located at the corners of the micropores (Figure 4a) and triggered the asymmetric collapse with the meniscus touched and coalesced with them (Figure 4b,c). Below, we present further experimental evidence to validate this hypothesis and the genesis of the microdroplets.

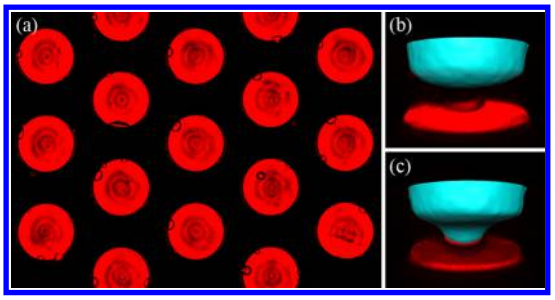

Figure 4. (a) Droplet-like features were commonly located at the corners of the pores. (b) A 3D image demonstrates the presence of the droplet immediately prior to contact with the progressing meniscus. (c) Coalescence between the meniscus and the droplet.

We placed a rhodamine-labeled droplet in the volume of 0.2 mL on the sample surface under 1 atm and room temperature. A 20× water immersion objective was used for observation. Once the sample was covered with water, circles similar to that in Figure 3f appeared immediately on the pore bottom. These features swelled spontaneously and even coalesced with the ones (indicated by arrows "1" in Figure 5) within the same micropore. Figure 5 shows the representative morphology of collapse-triggering circles. Occasionally, some circles expanded eventually to cover the entire bottom of a micropore (indicated by arrow "2" in Figure 5). For those cases, we subsequently took a time series of images of the same micropore along the pore center plane in line scan mode (the second row of Figure 5). The reflected interface (indicated by arrows "3") indicates that it is the upper boundary of the feature growing from the pore bottom. This boundary proceeded to advance to the upper water−air interface pinned at the top corner of the micropore. Eventually, the two interfaces coalesced, which was followed by

DOI: 10.1021/la503465q
Langmuir XXXX, XXX, XXX−XXX

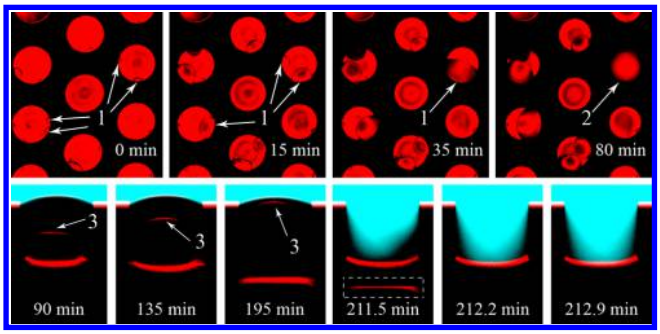

Figure 5. Top row: formation and morphology of partial-circular features from the top view of a water-covered sample. Bottom row: confocal microscopy (line scan) of the case indicated by "2" in the top row. Because the scan direction is from bottom to top, the image in the dashed box at 211.5 min was actually reflective signals of the pore bottom immediately before the coalescence of the interfaces. As soon as the coalescence occurred (212.2 min), the reflective image disappeared.

a quick diffusion of the rhodamine molecules downward from the water above into the entire space of the micropore within 1 min (beginning at the time 211.5 min). The time scale is consistent with the diffusion time of Rhodamine B (diffusion coefficient $D \sim 4.27 \times 10^{-10}$ m^2/s in water at 25 °C[56]). In contrast, as soon as water droplet atop the sample was sucked away so that the micropores were exposed to the ambient air, the partial-circular features quickly disappeared. The above observations strongly suggest that these partial circles are nothing but microdroplets condensed on the pore bottom. Prior to merging with rhodamine-labeled water body, the droplets were fluorescence-free, suggesting that they were not results of "trickling" from the main body. Postmerging, the diffusive process validates that those features were in an aqueous state.

In the next step, we establish that these microdroplets resulted from impurities on the sample. Figure 6a is a scanning electron microscopy (SEM) image taken in dry condition prior to water coverage, and the impurities are indicated by numbers. In Figure 6b, evidently microdroplets grew on these sites, which are also indicated by numbers corresponding to those in Figure 6a. It is reasonable to speculate that the microdroplets formed via the condensation of vapor in the micropores, and the impurities played the role of nuclei. As water covered the sample, the vapor density in the closed micropores would increase due to evaporation at the water−air interfaces, leading to oversaturation and hence condensation on the impurities.[57−61] The most probable source of the impurities is from prior use. The unavoidable impurities suspended in water deposited on the pore bottom during evaporation after full wetting of the micropores.[62,63] Although after each use the sample was dipped in ethanol for 1 day for cleaning, the impurities could not be effectively removed (Figure 6a) and accumulated with the number of use. Indeed, in the six experiments where symmetric collapses were observed, all samples were of the first use. In contrast, for the 48 experiments where asymmetric collapses and the corresponding microdroplets were observed, the samples were reused after prior water immersion.

The above results strongly purport that microdroplets formed from impurities, especially those derived from prior use, are a major triggering source for asymmetric collapse. A brief discussion in the context of prior work is appropriate here.

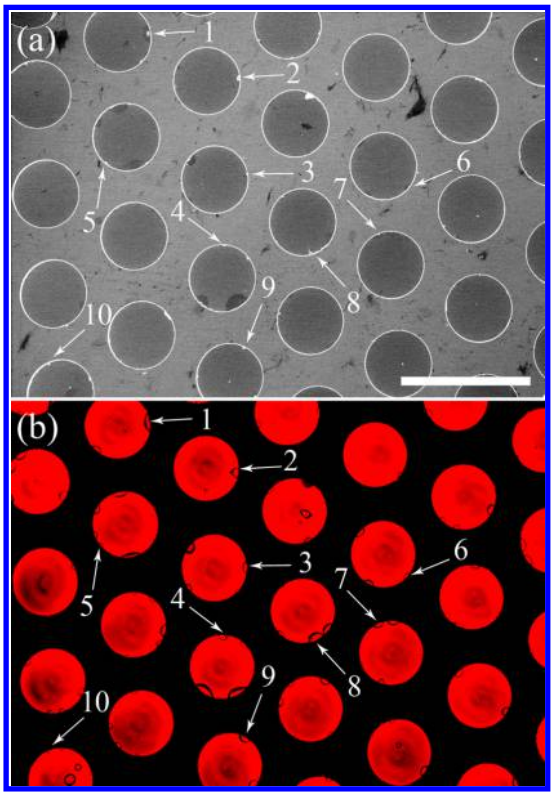

Figure 6. Comparison between the SEM image (a) showing the impurities and the confocal image (b) showing the microdroplets at the same location on the pore bottom. The impurity sites and the corresponding droplets are labeled with the same number in (a) and (b), respectively. The scale bar is 100 μm.

In an energy-based continuum theory by Giacomello et al.,[53,54] asymmetric collapse is predicted to occur in the absence of triggering impurities if the asymmetric state assumes a favorable (lower) energy. In our work, asymmetric collapse occurred exclusively with triggering microdroplets. In their absence, symmetric collapse occurred instead. We speculate that this is most probably due to that in our specific configuration the system could not overcome the energy barrier to reach the asymmetric state and hence remained symmetric in the "touchdown". However, once the impurity sites were present, the energy barrier was lowered, and the asymmetric state can be achieved. We also note that the model by Giacomello et al. includes a few idealizations; e.g., the gas in the cavity is treated as vapor at constant pressure, and the diffusive process is ignored. A more accurate model thus needs to be developed to predict asymmetric collapse and is not included in the current work.

Asymmetric collapses shorten the progression of the metastable state and hence affect the lifespan of and the ability to recover superhydrophobicity. In the representative case shown in Figure 3, the time to "touchdown" in asymmetric collapse reduced by 46% when compared with that in the symmetric case. Avoiding asymmetric collapse is thus advantageous for the maintenance of superhydrophobicity. We propose that the hierarchical structure can be an effective remedy, and a preliminary study is presented below as the last part of current work. Based on the single-level microstructured surface used above, nanosized pillars on which smaller steps grew were fabricated on the bottom of the micropores using the method of black silicon (Figure 2c). Following the same procedure, we

DOI: 10.1021/la503465q
Langmuir XXXX, XXX, XXX−XXX

immersed the hierarchical structured sample underwater and applied a constant pressure of 50 kPa to observe the collapse process. We performed 10 experiments with hierarchical structures that have been reused. Figure 7 shows the representative collapse process. No asymmetric collapse was observed for all cases examined, nor did we detect the presence of the triggering microdroplets. We believe the avoidance of microdroplets on hierarchical structures owes to the ability to remove the impurities. After each use, the sample was dipped in ethanol for 1 day in an identical protocol to that of the single-level samples, and impurities were effectively washed away due to the superhydrophobicity of the nanopillar array. This effect is known as self-cleaning.[5,6] Thus, there were much fewer impurities left on the pore bottom of the hierarchical structured surfaces before the next experiment, leading to negligible production of residue microdroplets. Asymmetric collapse, along with the significant shortening of the metastable state associate with it, is therefore effectively eliminated, increasing the lifespan of the sample. Furthermore, the benefit of a hierarchical structure extends beyond the annihilation of the asymmetric collapse. Even after the microscale Wenzel state (i.e., the microscopically observed touchdown) is fully reached, the nanoscale features may still remain in a Cassie state, which is termed the "nano-Cassie" state. According to scaling laws we derived earlier,[49] the lifespan of the metastable state scales inversely with the pore radius. Hierarchical structures can hence greatly enhance the lifetime of the submerged structured surfaces to several tens of hours[17] due to the nano-Cassie state, compared with the several tens of minutes on the surfaces with single-level microstructures.

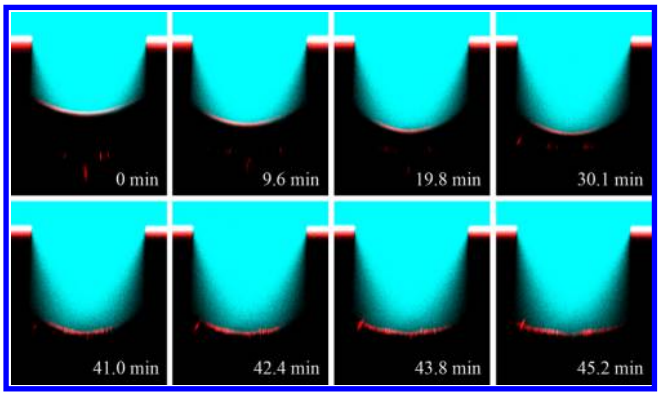

Figure 7. Representative symmetric collapse on a submerged hierarchically structured surface.

CONCLUSIONS

In conclusion, we used confocal microscopy to observe the last stage of the CB–W transition, namely, the "collapse". Both symmetric and asymmetric collapses were captured *in situ* on surfaces patterned with cylindrical micropores. Asymmetric collapses significantly shorten the duration of the metastable state and hence affect the lifetime of superhydrophobicity. We found that the asymmetric collapse was induced by impurities due to prior use of the samples. Proper cleaning of the surface is thus of general importance to ensure consistent functioning of these structured devices. We propose that the use of hierarchical structure can effectively address this problem by harnessing its self-cleaning property. The current work offers an in-depth understanding of the CB–W transition and can benefit design explorations to enhance the longevity of structured superhydrophobicity.

ASSOCIATED CONTENT

Supporting Information

3D movies of both symmetric and asymmetric collapses animating the dynamic process. This material is available free of charge via the Internet at http://pubs.acs.org.

AUTHOR INFORMATION

Corresponding Authors

*E-mail hlduan@pku.edu.cn (H.D.).
*E-mail hlin@jove.rutgers.edu (H.L.).

Notes

The authors declare no competing financial interest.

ACKNOWLEDGMENTS

We acknowledge the Major State Basic Research Development Program of China (Grant 2011CB013101) and the National Natural Science Foundation of China (NSFC) under Grants 11225208 and 11172001. Hao Lin acknowledges support from NSF CBET-0747886. Huiling Duan would like to acknowledge the Alexander von Humboldt (AvH) foundation in Germany to support this work through project "Mechanics theory of materials with complex surfaces and its applications" in the frame of the AvH program for funding a research group linkage.

REFERENCES

(1) Nosonovsky, M.; Bharat, B. Superhydrophobic Surfaces and Emerging Applications: Non-Adhesion, Energy, Green Engineering. *Curr. Opin. Colloid Interface Sci.* **2009**, *14*, 270–280.
(2) Zhang, X.; Shi, F.; Niu, J.; Jiang, Y.; Wang, Z. Superhydrophobic Surfaces: from Structural Control to Functional Application. *J. Mater. Chem.* **2008**, *18*, 621–633.
(3) Miljkovic, N.; Wang, E. N. Condensation Heat Transfer on Superhydrophobic Surfaces. *MRS Bull.* **2013**, *38*, 397–406.
(4) Xue, Y. H.; Yuan, H. J.; Su, W. D.; Shi, Y. P.; Duan, H. L. Enhanced Load-Carrying Capacity of Hairy Surfaces Floating on Water. *Proc. R. Soc., Sect. A: Math. Phys. Eng. Sci.* **2014**, *470*, 20130832.
(5) Feng, L.; Li, S. H.; Li, Y. S.; Li, H. J.; Zhang, L. J.; Zhai, J.; Song, Y. L.; Liu, B. Q.; Jiang, L.; Zhu, D. B. Super-Hydrophobic Surfaces: from Natural to Artificial. *Adv. Mater.* **2002**, *14*, 1857–1860.
(6) Kota, A. K.; Li, Y. X.; Mabry, J. M.; Tuteja, A. Hierarchically Structured Superoleophobic Surfaces with Ultralow Contact Angle Hysteresis. *Adv. Mater.* **2012**, *24*, 5838–5843.
(7) Rothstein, J. P. Slip on Superhydrophobic Surfaces. *Annu. Rev. Fluid Mech.* **2010**, *42*, 89–109.
(8) Vinogradova, O. I.; Belyaev, A. V. Wetting, Roughness and Flow Boundary Conditions. *J. Phys.: Condens. Matter* **2011**, *23*, 184104.
(9) Byun, D.; Kim, J.; Ko, H. S.; Park, H. C. Direct Measurement of Slip Flows in Superhydrophobic Microchannels with Transverse Grooves. *Phys. Fluids* **2008**, *20*, 113601.
(10) Wu, Y.; Xue, Y. H.; Pei, X. W.; Cai, M. R.; Duan, H. L.; Huck, W. T. S.; Zhou, F.; Xue, Q. J. Adhesion-Regulated Switchable Fluid Slippage on Superhydrophobic Surfaces. *J. Phys. Chem. C* **2014**, *118*, 2564–2569.
(11) Cassie, A. B. D.; Baxter, S. Wettability of Porous Surfaces. *Trans. Faraday Soc.* **1944**, *40*, 546–550.
(12) Bormashenko, E.; Pogreb, R.; Whyman, G.; Erlich, M. Resonance Cassie-Wenzel Wetting Transition for Horizontally Vibrated Drops Deposited on a Rough Surface. *Langmuir* **2007**, *23*, 12217–12221.
(13) Reyssat, M.; Yeomans, J. M.; Quéré, D. Impalement of Fakir Drops. *Eur. Phys. Lett.* **2008**, *81*, 26006.

DOI: 10.1021/la503465q
Langmuir XXXX, XXX, XXX–XXX

(14) Tsai, P. C.; Lammertink, R. G. H.; Wessling, M.; Lohse, D. Evaporation-Triggered Wetting Transition for Water Droplets upon Hydrophobic Microstructures. *Phys. Rev. Lett.* **2010**, *104*, 116102.
(15) Chen, X. M.; Ma, R. Y.; Li, J. T.; Hao, C. L.; Guo, W.; Luk, B. L.; Li, S. C.; Yao, S. H.; Wang, Z. K. Evaporation of Droplets on Superhydrophobic Surfaces: Surface Roughness and Small Droplet Size Effects. *Phys. Rev. Lett.* **2012**, *109*, 116101.
(16) Bobji, M. S.; Kumar, S. V.; Asthana, A.; Govardhan, R. N. Underwater Sustainability of the "Cassie" State of Wetting. *Langmuir* **2009**, *25*, 12120−12126.
(17) Poetes, R.; Holtzmann, K.; Franze, K.; Steiner, U. Metastable Underwater Superhydrophobicity. *Phys. Rev. Lett.* **2010**, *105*, 166104.
(18) Samaha, M. A.; Tafreshi, H. V.; Gad-el-Hak, M. Sustainability of Superhydrophobicity under Pressure. *Phys. Fluids* **2012**, *24*, 112103.
(19) Lafuma, A.; Quéré, D. Superhydrophobic States. *Nat. Mater.* **2003**, *2*, 457−460.
(20) Xue, Y. H.; Chu, S. G.; Lv, P. Y.; Duan, H. L. Importance of Hierarchical Structures in Wetting Stability on Submersed Superhydrophobic Surfaces. *Langmuir* **2012**, *28*, 9440−9450.
(21) Shahraz, A.; Borhan, A.; Fichthorn, K. A. A Theory for the Morphological Dependence of Wetting on a Physically Patterned Solid Surface. *Langmuir* **2012**, *28*, 14227−14237.
(22) Bormashenko, E.; Bormashenko, Y.; Stein, T.; Whyman, G.; Pogreb, R. Environmental Scanning Electron Microscopy Study of the Fine Structure of the Triple Line and Cassie-Wenzel Wetting Transition for Sessile Drops Deposited on Rough Polymer Substrates. *Langmuir* **2007**, *23*, 4378−4382.
(23) Krupenkin, T. N.; Taylor, J. A.; Wang, E. N.; Kolodner, P.; Hodes, M.; Salamon, T. R. Reversible Wetting-Dewetting Transitions on Electrically Tunable Superhydrophobic Nanostructured Surfaces. *Langmuir* **2007**, *23*, 9128−9133.
(24) Xue, Y. H.; Markmann, J.; Duan, H. L.; Weissmüller, J.; Huber, P. Switchable Imbibition in Nanoporous Gold. *Nat. Commun.* **2014**, *5*, 4237.
(25) Bartolo, D.; Bouamrirene, F.; Verneuil, E.; Buguin, A.; Silberzan, P.; Moulinet, S. Bouncing or Sticky Droplets: Impalement Transitions on Superhydrophobic Micropatterned Surfaces. *Eur. Phys. Lett.* **2006**, *74*, 299−305.
(26) Kwon, H. M.; Paxson, A. T.; Varanasi, K. K.; Patankar, N. A. Rapid Deceleration-Driven Wetting Transition during Pendant Drop Deposition on Superhydrophobic Surfaces. *Phys. Rev. Lett.* **2011**, *106*, 036102.
(27) Wenzel, R. N. Resistance of Solid Surfaces to Wetting by Water. *Ind. Eng. Chem.* **1936**, *28*, 988−994.
(28) Moulinet, S.; Bartolo, D. Life and Death of a Fakir Droplet: Impalement Transitions on Superhydrophobic Surfaces. *Eur. Phys. J. E* **2007**, *24*, 251−260.
(29) Forsberg, P.; Nikolajeff, F.; Karlsson, M. Cassie−Wenzel and Wenzel−Cassie Transitions on Immersed Superhydrophobic Surfaces under Hydrostatic Pressure. *Soft Matter* **2011**, *7*, 104−109.
(30) Xu, X. M.; Vereecke, G.; Chen, C.; Pourtois, G.; Armini, S.; Verellen, N.; Tsai, W. K.; Kim, D. W.; Lee, E.; Lin, C. Y.; Van Dorpe, P.; Struyf, H.; Holsteyns, F.; Moshchalkov, V.; Indekeu, J.; De Gendt, S. Capturing Wetting States in Nanopatterned Silicon. *ACS Nano* **2014**, *8*, 885−893.
(31) Rathgen, H.; Mugele, F. Microscopic Shape and Contact Angle Measurement at a Superhydrophobic Surface. *Faraday Discuss.* **2010**, *146*, 49−56.
(32) Lei, L.; Li, H.; Shi, J.; Chen, Y. Diffraction Patterns of a Water-Submerged Superhydrophobic Grating under Pressure. *Langmuir* **2009**, *26*, 3666−3669.
(33) Checco, A.; Ocko, B. M.; Rahman, A.; Black, C. T.; Tasinkevych, M.; Giacomello, A.; Dietrich, S. Collapse and Reversibility of the Superhydrophobic State on Nanotextured Surfaces. *Phys. Rev. Lett.* **2014**, *111*, 216101.
(34) Papadopoulos, P.; Deng, X.; Mammen, L.; Drotlef, D. M.; Battagliarin, G.; Li, C.; Muellen, K.; Landfester, K.; del Campo, A.; Butt, H. J.; Vollmer, D. Wetting on the Microscale: Shape of a Liquid Drop on a Microstructured Surface at Different Length Scales. *Langmuir* **2012**, *28*, 8392−8398.
(35) Papadopoulos, P.; Mammen, L.; Deng, X.; Vollmer, D.; Butt, H. J. How Superhydrophobicity Breaks Down. *Proc. Natl. Acad. Sci. U. S. A.* **2013**, *110*, 3254−3258.
(36) Luo, C.; Zheng, H.; Wang, L.; Fang, H. P.; Hu, J.; Fan, C. H.; Cao, Y.; Wang, J. A. Direct Three-Dimensional Imaging of the Buried Interfaces between Water and Superhydrophobic Surfaces. *Angew. Chem., Int. Ed.* **2010**, *49*, 9145−9148.
(37) Verho, T.; Korhonen, J. T.; Sainiemi, L.; Jokinen, V.; Bower, C.; Franze, K.; Franssila, S.; Andrew, P.; Ikkala, O.; Ras, R. H. A. Reversible Switching between Superhydrophobic States on a Hierarchically Structured Surface. *Proc. Natl. Acad. Sci. U. S. A.* **2012**, *109*, 10210−10213.
(38) Tsai, P. C.; Peters, A. M.; Pirat, C.; Wessling, M.; Lammertink, R. G. H.; Lohse, D. Quantifying Effective Slip Length over Micropatterned Hydrophobic Surfaces. *Phys. Fluids* **2009**, *21*, 112002.
(39) Patankar, N. A. Transition between Superhydrophobic States on Rough Surfaces. *Langmuir* **2004**, *20*, 7097−7102.
(40) David, R.; Neumann, A. W. Energy Barriers between the Cassie and Wenzel States on Random, Superhydrophobic Surfaces. *Colloids Surf., A* **2013**, *425*, 51−58.
(41) Bormashenko, E.; Musin, A.; Whyman, G.; Zinigrad, M. Wetting Transitions and Depinning of the Triple Line. *Langmuir* **2012**, *28*, 3460−3464.
(42) Ren, W. Q. Wetting Transition on Patterned Surfaces: Transition States and Energy Barriers. *Langmuir* **2014**, *30*, 2879−2885.
(43) Blow, M. L.; Yeomans, J. M. Superhydrophobicity on Hairy Surfaces. *Langmuir* **2010**, *26*, 16071−16083.
(44) Dupuis, A.; Yeomans, J. M. Modeling Droplets on Superhydrophobic Surfaces: Equilibrium States and Transitions. *Langmuir* **2005**, *21*, 2624−2629.
(45) Lobaton, E. J.; Salamon, T. R. Computation of Constant Mean Curvature Surfaces: Application to the Gas-Liquid Interface of a Pressurized Fluid on a Superhydrophobic Surface. *J. Colloid Interface Sci.* **2007**, *314*, 184−198.
(46) Zheng, Q. S.; Yu, Y.; Zhao, Z. H. Effects of Hydraulic Pressure on the Stability and Transition of Wetting Modes of Superhydrophobic Surfaces. *Langmuir* **2005**, *21*, 12207−12212.
(47) Emami, B.; Tafreshi, H. V.; Gad-el-Hak, M.; Tepper, G. C. Effect of Fiber Orientation on Shape and Stability of Air-Water Interface on Submerged Superhydrophobic Electrospun Thin Coatings. *J. Appl. Phys.* **2012**, *111*, 064325.
(48) Emami, B.; Tafreshi, H. V.; Gad-el-Hak, M.; Tepper, G. C. Predicting Shape and Stability of Air-Water Interface on Superhydrophobic Surfaces Comprised of Pores with Arbitrary Shapes and Depths. *Appl. Phys. Lett.* **2012**, *100*, 013104.
(49) Lv, P. Y.; Xue, Y. H.; Shi, Y. P.; Lin, H.; Duan, H. L. Metastable States and Wetting Transition of Submerged Superhydrophobic Structures. *Phys. Rev. Lett.* **2014**, *112*, 196101.
(50) Patankar, N. A. Consolidation of Hydrophobic Transition Criteria by Using an Approximate Energy Minimization Approach. *Langmuir* **2010**, *26*, 8941−8945.
(51) Ishino, C.; Okumura, K.; Quéré, D. Wetting Transitions on Rough Surfaces. *Eur. Phys. Lett.* **2004**, *68*, 419−425.
(52) Whyman, G.; Bormashenko, E. How to Make the Cassie Wetting State Stable? *Langmuir* **2011**, *27*, 8171−8176.
(53) Giacomello, A.; Meloni, S.; Chinappi, M.; Casciola, C. M. Cassie-Baxter and Wenzel States on a Nanostructured Surface: Phase Diagram, Metastabilities, and Transition Mechanism by Atomistic Free Energy Calculations. *Langmuir* **2012**, *28*, 10764−10772.
(54) Giacomello, A.; Chinappi, M.; Meloni, S.; Casciola, C. M. Metastable Wetting on Superhydrophobic Surfaces: Continuum and Atomistic Views of the Cassie-Baxter−Wenzel Transition. *Phys. Rev. Lett.* **2012**, *109*, 226102.
(55) 3D movies of both symmetric and asymmetric collapses animating the dynamic process are in the Supporting Information.

DOI: 10.1021/la503465q
Langmuir XXXX, XXX, XXX−XXX

(56) Culbertson, C. T.; Jacobson, S. C.; Ramsey, J. M. Diffusion Coefficient Measurements in Microfluidic Devices. *Talanta* **2002**, *56*, 365−373.
(57) Varanasi, K. K.; Hsu, M.; Bhate, N.; Yang, W. S.; Deng, T. Spatial Control in the Heterogeneous Nucleation of Water. *Appl. Phys. Lett.* **2009**, *95*, 094101.
(58) Narhe, R. D.; Beysens, D. A. Nucleation and Growth on a Superhydrophobic Grooved Surface. *Phys. Rev. Lett.* **2004**, *97*, 076103.
(59) Hu, H.; Larson, R. G. Evaporation of a Sessile Droplet on a Substrate. *J. Phys. Chem. B* **2002**, *106*, 1334−1344.
(60) Tay, A.; Monteux, C.; Bendejacq, D.; Lequeux, F. How a Coating Is Hydrated Ahead of the Advancing Contact Line of a Volatile Solvent Droplet. *Eur. Phys. J. E* **2010**, *33*, 203−210.
(61) Ruckenstein, E.; Berim, G. O. Kinetics of Heterogeneous Nucleation on a Rough Surface: Nucleation of a Liquid Phase in Nanocavities. *J. Colloid Interface Sci.* **2010**, *351*, 277−282.
(62) Deegan, R. D.; Bakajin, O.; Dupont, T. F.; Huber, G.; Nagel, S. R.; Witten, T. A. Capillary Flow as the Cause of Ring Stains from Dried Liquid Drops. *Nature* **1997**, *389*, 827−829.
(63) Yunker, P. J.; Still, T.; Lohr, M. A.; Yodh, A. G. Suppression of the Coffee-Ring Effect by Shape-Dependent Capillary Interactions. *Nature* **2011**, *476*, 308−311.

DOI: 10.1021/la503465q
Langmuir XXXX, XXX, XXX−XXX